Available online at www.sciencedirect.com
SCIENCE DIRECT®
Journal of Solid State Chemistry 171 (2003) 69–75
JOURNAL OF SOLID STATE CHEMISTRY
http://elsevier.com/locate/jssc

Orbital degrees of freedom and ordering phenomena in a 4*f* system

M. Amara,[a,*] S.E. Luca,[a] R.M. Galéra,[a] I. Aviani,[b] and J.F. Bérar[c]

[a] *Laboratoire Louis-Néel, C.N.R.S., BP 166X, Grenoble, Cedex F-38042, France*
[b] *Institute of Physics, Bijenicka cesta 46, POB 304, Zagreb HR-10000, Croatia*
[c] *Laboratoire de Cristallographie, C.N.R.S., BP 166X, Grenoble F-38042, France*

Received 8 May 2002; received in revised form 1 July 2002; accepted 11 November 2002

Abstract

Due to orbital degeneracy, a 4*f* electronic shell has the ability to distort when influenced by an electrostatic, magnetic or collective intersite field. In case of collective phenomena, the 4*f* asphericity which develops may result in a strain mode and/or introduce a new charge periodicity. The first is accessible via dilatometric techniques whereas the second needs a microscopic probe, X-rays, to be detected.

To illustrate the efficiency of these techniques for sensing the 4*f* asphericity, the study of NdMg's collinear and multiaxial phases is introduced.

Keywords: Quadrupolar; Orbital; Antiferromagnetism; X-ray; Magnetostriction

1. Introduction

Except for gadolinium, the ground state of a rare-earth atom carries an orbital degeneracy in addition to the magnetic one. This results in the ability for the electronic shell to distort when submitted to an anisotropic electrostatic or magnetic influence. In a crystal, the orbital degeneracy is partly lifted by the crystalline electric field: the less symmetric the site occupied by the rare-earth, the lower the degeneracy of the crystal field levels. Therefore, orbital effects are more pronounced in systems where a highly symmetrical crystal field preserves a large orbital degeneracy. This is particularly true in the case of cubic systems for which no quadrupolar 4*f* moment can result from the crystal field.

With the availability of orbital degrees of freedom, orbital phenomena of single site or collective nature are to be expected. Single site phenomena can be most carefully investigated within the orbitally/magnetically disordered state and will not be further considered here. Regarding the collective phenomena, one has to distinguish between two main situations [1,2]:

(i) the orbital degeneracy, through an effective couplings between orbitals, is the driving mechanism of the ordering. This is the case of the so-called cooperative Jahn–Teller (JT) effect which is to be expected as soon as the crystal field ground state degeneracy is higher than the Kramers minimum. Then the rare-earth site symmetry is collectively lowered by a strain mode and the 4*f* shells assume a new shape. In some cases, the dominant orbital coupling does not result from a strain mode but is mediated by electrons or phonons (non-JT). The most general definition of such ordering situations, JT or non-JT, is that of a quadrupolar ordering.

(ii) the orbital degeneracy is reduced as a consequence of an ordering whose primary order parameter is not of orbital nature. This is by far the most common situation for rare-earth metallic compounds in which a magnetic order usually develops at temperatures higher than any potential quadrupolar order. However, the couplings between quadrupoles may play a significant role within the magnetically ordered states. They have been proven to determine the multiaxial nature of magnetic structures or to influence the magnetic transitions, both in type (from second to first order) and critical temperature or field [3].

The two points above underscore the critical importance of the 4*f* orbital arrangements in the ordering mechanisms of rare-earth compounds. Determining the

*Corresponding author. Fax: +33-4-76-88-11-91.
E-mail address: amara@polycnrs-gre.fr (M. Amara).

0022-4596/03/$ - see front matter © 2003 Elsevier Science (USA). All rights reserved.
doi:10.1016/S0022-4596(02)00147-0

4*f* distribution within the ordered state should provide valuable information for characterising the order at the microscopic scale and identifying the role of the orbital couplings. This is difficult to achieve experimentally, as this requires detection of a slight deviation from sphericity for an inner electronic shell. A few techniques may be, however, considered in view of such an investigation.

In the paramagnetic state, due to the single site behaviour, spectroscopic techniques can provide one with the crystal electric field energy scheme. Then, from a single site approach, using a quantum description of the atom, one can determine the 4*f* aspherical distribution resulting from the crystal field.

Unfortunately, due to the variety of collective excitations which may occur, such an approach cannot be extended to a magnetically or orbitally ordered state. In that case, if the changes in the asphericity propagate at the centre of the Brillouin zone ($\boldsymbol{q} = \mathbf{0}$), the coupling of the 4*f* shell with the lattice (magnetoelastic coupling) provides a means to access the quadrupoles values via macroscopic (dilatometry) or diffraction (X-ray, neutron diffraction) techniques. Such techniques are useless if the 4*f* asphericity develops periodically ($\boldsymbol{q} \neq \mathbf{0}$) as then the strain should cancel. In this case the only effective probe remains X-rays, which directly couple to the 4*f* shell electronic distribution. In concomitance with the magnetic/orbital ordering, extra diffraction peaks related to 4*f* multipoles should appear in agreement with the new charge periodicity of the system.

To illustrate these techniques and analyses, an investigation of NdMg magnetically ordered phases is here introduced.

2. Principles

2.1. Quadrupolar moments

In the description of the 4*f* shell, the Hartree–Fock like potential determines a same radial distribution for all 4*f* electrons. To the relevant orders of perturbation, the rare-earth environment acts only on the angular distribution and the radial part will not be further considered here. For a rare-earth ion located at a site which has the inversion symmetry, this angular distribution can be decomposed into a sum of even order spherical harmonics. For the cubic symmetry considered here, the main changes in the 4*f* asphericity will appear at the second order, that is for the "quadrupolar" part, $\rho_2(\theta,\varphi)$, of the angular distribution. Fourth and sixth order terms, which are already ordered by the crystal field, are not expected to be significantly affected by the ordering phenomena. Instead of using spherical harmonics, the $\rho_2(\theta,\varphi)$ distribution is written here using a basis of real angular, orthogonal, functions (see Table 1 for their definitions) which correspond to the usual quadrupolar operators:

$$\rho_2(\theta,\varphi) = c_2^0 Q_2^0(\theta,\varphi) + c_2^2 Q_2^2(\theta,\varphi) + c_{xy} Q_{xy}(\theta,\varphi) + c_{yz} Q_{yz}(\theta,\varphi) + c_{zx} Q_{zx}(\theta,\varphi).$$

To obtain the c_l^m coefficients of the expansion, five normalised scalar products are to be expressed. For instance

$$c_2^0 = \frac{5}{16\pi} \int\int_{\theta,\varphi} Q_2^0(\theta,\varphi)\rho_2(\theta,\varphi)\, sin\,\theta\, d\theta\, d\varphi.$$

In a quantum description of the 4*f* shell (the method is detailed by Schmitt in Ref. [4]), the $\rho_2(\theta,\varphi)$ distribution results from a thermal average over *n*-electrons wave functions. Each eigenstate contributes to $\rho_2(\theta,\varphi)$ through the square modulus of its angular wave function times a Boltzmann factor. The angular integrals defining the c_l^m coefficients can be then identified with matrix elements of *n*-electrons angular operators as listed in Table 1. Using Stevens' equivalent operators method, such integrals are reduced to matrix elements of total spin operators [5]. These equivalent operators are reported in Table 1, as well as the

Table 1
The quadrupolar angular functions, their associated *n*-electron angular and Stevens equivalents operator. The last column gives the expressions for the angular distribution expansion coefficients (see text). The summations are over the 4*f* electrons and α_J is the Stevens second order multiplying factor

Real angular function	*n*-electrons operator	Equivalent operator	Distribution coefficient
$Q_2^0 = 4\sqrt{\frac{\pi}{5}}\, Y_2^0(\theta,\varphi)$	$\hat{Q}_2^0 = \sum_{j=1}^n Q_2^0(\theta_j,\varphi_j)$	$\alpha_J\left[3J_z^2 - J(J+1)\right] = \alpha_J O_2^0$	$c_2^0 = \frac{5}{16\pi}\alpha_J \langle O_2^0 \rangle$
$Q_2^2(\theta,\varphi) = \sqrt{\frac{8\pi}{15}}[Y_2^2(\theta,\varphi) + Y_2^{-2}(\theta,\varphi)]$	$\hat{Q}_2^2 = \sum_{j=1}^n Q_2^2(\theta_j,\varphi_j)$	$\alpha_J\left[J_x^2 - J_y^2\right] = \alpha_J O_2^2$	$c_2^2 = \frac{15}{16\pi}\alpha_J \langle O_2^2 \rangle$
$Q_{xy}(\theta,\varphi) = \mathrm{i}\sqrt{\frac{2\pi}{15}}[Y_2^{-2}(\theta,\varphi) - Y_2^2(\theta,\varphi)]$	$\hat{Q}_{xy} = \sum_{j=1}^n Q_{xy}(\theta_j,\varphi_j)$	$\alpha_J\left[\frac{J_xJ_y + J_yJ_x}{2}\right] = \alpha_J P_{xy}$	$c_{xy} = \frac{15}{4\pi}\alpha_J \langle P_{xy} \rangle$
$Q_{yz}(\theta,\varphi) = -\mathrm{i}\sqrt{\frac{2\pi}{15}}[Y_2^{-1}(\theta,\varphi) + Y_2^1(\theta,\varphi)]$	$\hat{Q}_{yz} = \sum_{j=1}^n Q_{yz}(\theta_j,\varphi_j)$	$\alpha_J\left[\frac{J_yJ_z + J_zJ_y}{2}\right] = \alpha_J P_{yz}$	$c_{yz} = \frac{15}{4\pi}\alpha_J \langle P_{yz} \rangle$
$Q_{zx}(\theta,\varphi) = \sqrt{\frac{2\pi}{15}}[Y_2^{-1}(\theta,\varphi) - Y_2^1(\theta,\varphi)]$	$\hat{Q}_{zx} = \sum_{i=1}^n Q_{zx}(\theta_j,\varphi_j)$	$\alpha_J\left[\frac{J_zJ_x + J_xJ_z}{2}\right] = \alpha_J P_{zx}$	$c_{zx} = \frac{15}{4\pi}\alpha_J \langle P_{zx} \rangle$

definitions which are then obtained for the angular distribution coefficients.

2.2. Magnetoelastic couplings

The magnetoelastic phenomena in rare-earth compounds are commonly described using a single-ion Hamiltonian and restricted to quadrupolar order. This term appears as a strain derivative of the crystal field term. For a cubic system this magnetoelastic Hamiltonian reads as

$$H_{me} = -B^{\gamma}(\varepsilon_1^{\gamma}O_2^0 + \sqrt{3}\varepsilon_2^{\gamma}O_2^2) - B^{\varepsilon}(\varepsilon_1^{\varepsilon}P_{xy} + \varepsilon_2^{\varepsilon}P_{yz} + \varepsilon_3^{\varepsilon}P_{zx}),$$

where the ε_n^{μ} are cubic symmetrised strains [6] and the B^{μ} the magnetoelastic couplings. This term has to compete with the elastic energy defined through the C_0^{μ} s background elastic constants. The strain being a macroscopic variable, its equilibrium value can be related to the statistical values of the quadrupolar operators by minimizing the free energy. For instance, the tetragonal strain mode is then linearly related to $\langle O_2^0 \rangle$:

$$\varepsilon_1^{\gamma} = \frac{2}{3}(\lambda_{\parallel} - \lambda_{\perp}) = \frac{B^{\gamma}}{C_0^{\gamma}}\langle O_2^0 \rangle \quad (1)$$

ε_1^{γ}, $\lambda_{\parallel}$ and $\lambda_{\perp}$ are the strains respectively parallel and perpendicular to the (Oz) fourfold axis.

The ratio B^{γ}/C_0^{γ} can be determined from magnetostriction measurements in the paramagnetic range (the so-called parastriction), using the linear high temperature part of the $H/\sqrt{\lambda_{\parallel} - \lambda_{\perp}}$ plot [7].

Measuring the strain is then a means for determining the value of $\langle O_2^0 \rangle$. The strain can be determined by measuring macroscopic length changes affecting the sample. The above expression of the strain, which is adapted to a single site treatment (in order to describe a paramagnetic situation for instance), has then to be adapted to ordered situations in which all rare-earth sites do not necessarily carry the same quadrupolar moments. In such cases the macroscopic strain can be related to the zone centre components only and therefore

$$\varepsilon_1^{\gamma} = \frac{B^{\gamma}}{C_0^{\gamma}}\langle O_2^0(\mathbf{0}) \rangle,$$

where $\langle O_2^0(\mathbf{0}) \rangle$ is the zone centre component of $\langle O_2^0 \rangle$. That is, for systems with a single site per cell, the average value of $\langle O_2^0 \rangle$ on the crystal.

2.3. Multipolar X-ray scattering

We consider the simple Thomson scattering of X-rays by the $4f$ electrons of a rare-earth ion. The scattering amplitude reduces to the Fourier transform of the electrons distribution over the atomic state. Decomposing this amplitude into a sum of terms related to the $4f$ multipolar operators, one obtains for the quadrupolar term (here in Thomson electron units) [8]

$$A_2(\mathbf{Q}) = \alpha_J F_2(Q)\left[\frac{1}{2}\left(3\frac{Q_z^2}{Q^2} - 1\right)\langle O_2^0 \rangle + \frac{3}{2}\left(\frac{Q_x^2 - Q_y^2}{Q^2}\right)\langle O_2^2 \rangle + 6\left(\frac{Q_x Q_y}{Q^2}\langle P_{xy} \rangle + cp\right)\right], \quad (2)$$

where $\mathbf{Q} = (Q_x Q_y Q_z)$ is the scattering vector, α_J the Stevens multiplying factor and $F_2(Q)$ the quadrupolar form factor which corresponds to a radial integral over the $4f$ electronic distribution $\rho(r)$:

$$F_2(Q) = \frac{5}{2}\int\left[\frac{3\cos(Qr)}{Q^2r^2} + \left(1 - \frac{3}{Q^2r^2}\right)\frac{\sin(Qr)}{Qr}\right]\rho(r)r^2\,\mathrm{d}r.$$

In contrast with the usual spherical scattering, this aspherical form factor cancels for $Q = 0$ and is maximum at intermediate scattering angles.

An X-ray reflection should then include a quadrupolar contribution, provided the scattering vector agrees with the quadrupolar wave vectors. However, the maximum contribution to the scattering amplitude is restricted to a few hundredths Thompson electrons which is not easy to detect. Actually, the quadrupolar scattered intensity may be observed only if not superimposed with a strong reflection. This is what will happen in case the ordering introduces a new charge periodicity related to quadrupolar wave vectors out from the zone centre. The X-ray scattering technique thus appears as complementary to the magnetostriction measurements which are sensitive to zone centre components only.

3. Application to NdMg

The CsCl-type compound NdMg orders antiferromagnetically at $T_N = 61\,K$ and displays a second magnetic transition at $T_R = 35\,K$. The transition at T_R corresponds to a change from a collinear structure (phase I, label I on Fig. 1), at high temperature, to a multiaxial one (phase II, label II on Fig. 1), at low temperature [9]. As it is clearly shown in Fig. 1, they determine a tetragonal symmetry lowering, only one fourfold symmetry axis being preserved in the ordered states. A more detailed analysis can be developed in order to explicit the $4f$ charge consequences of the magnetic order [10].

Within phase I, described by a unique wave vector [0 0 1/2] propagating a magnetic moment component along [0 0 1], only one quadrupolar component is ordered. At any j site

$$\langle O_2^0 \rangle_j = \langle O_2^0(\mathbf{0}) \rangle = Q_0.$$

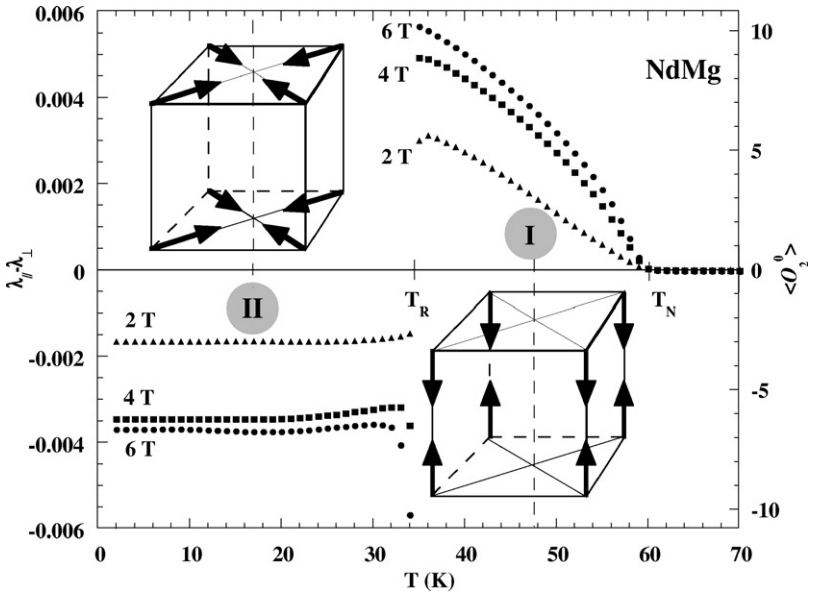

Fig. 1. The spontaneous tetragonal strain of NdMg measured under magnetic fields of 2, 4 and 6 T (see text for the field orientation). The inserted drawings are sketches of the magnetic structures in phases I and II. The right scales give directly the $\langle O_2^0 \rangle$ value (see text).

Phase II, is multiaxial, being described by two Fourier components: $\boldsymbol{m_1} = [1/\sqrt{2}\,0\,0]$,with wave vectors $\boldsymbol{k_1} = [1/2\,0\,0]$ and $\boldsymbol{m_2} = [0\,1/\sqrt{2}\,0]$, with wave vector $\boldsymbol{k_2} = [0\,1/2\,0]$. One can deduce that, for the j site located at $\boldsymbol{R}_j$, two quadrupolar components are ordered:

$$\langle O_2^0 \rangle_j = \langle O_2^0(\mathbf{0}) \rangle = -\tfrac{1}{2}Q_0,$$

$$\langle P_{xy} \rangle_j = \tfrac{1}{4}[Q_0 - Q_1]e^{i\boldsymbol{q}\boldsymbol{R}_j} = \langle P_{xy}(\boldsymbol{q}) \rangle e^{i\boldsymbol{q}\boldsymbol{R}_j}$$
$$\text{with } \boldsymbol{q} = [1/2\,1/2\,0]. \quad (3)$$

The zone centre component is the same $\langle O_2^0 \rangle$ in the two phases, but with an opposite sign. The so defined tetragonal strain mode (see Eq. (1)) should also change sign at T_R.

A zone boundary components $\langle P_{xy}(\boldsymbol{q}) \rangle$, potentially detected by X-ray diffraction, exists only in phase II, with wave vector [1/2 1/2 0].

3.1. Measurement of spontaneous magnetostriction

The lattice symmetry lowering which develops at the onset of a magnetic and/or orbital order determines the partitioning of the sample into domains. The apparent sample strain tends to cancel and no reliable information can be obtained from dilatometric measurements. To overcome this difficulty, one has to act on the domain partition through some external stress. On a magnetic system, applying a magnetic field is more practical and versatile (in direction) than applying a mechanical stress. Indeed, for a given direction of the applied field the magnetostriction domains should have different energies. This is obvious in case of a ferromagnetic order but also applies for antiferromagnetic or quadrupolar order via the magnetic first-order susceptibility tensor.

Acting through differences in susceptibility is a priori less effective than playing directly with the ferromagnetic components. It may require rather high magnetic fields and the ability of rotating the sample (or field) in order to get a maximum susceptibility contrast between domains. These are two features of the magnetostriction setup in the Louis–Néel laboratory. This apparatus uses the capacitance method for magnetostriction measurements in the temperature range 1.5–300 K and in magnetic fields up to 6.5 T. As a result of a vertical rotation axis, the angle between the probed sample direction and the horizontal field can be adjusted between 0° and 360°.

To characterise the tetragonal magnetostriction modes of NdMg, one has to determine the relative changes in length, $\lambda_{\parallel}$ and $\lambda_{\perp}$, respectively parallel and perpendicular to the preserved fourfold axis. Two phases, I and II, are to be investigated and therefore four different strains need to be measured: $\lambda_{\perp}(\mathrm{I})$, $\lambda_{\parallel}(\mathrm{I})$, $\lambda_{\parallel}(\mathrm{II})$ and $\lambda_{\perp}(\mathrm{II})$.

As the system becomes tetragonal instead of cubic, the magnetic first order susceptibility is no longer isotropic and is defined by two independent values: $\chi_{\parallel}$ and $\chi_{\perp}$, the susceptibilities respectively parallel and perpendicular to the fourfold axis. In an antiferromagnet, the maximum susceptibility is obtained for a field acting perpendicularly to the magnetic moment direction. Thus, in phase I, where the magnetic moments are parallel to the fourfold axis, one can expect that $\chi_{\parallel} < \chi_{\perp}$ whereas, in phase II, in which moments are perpendicular to the fourfold axis, $\chi_{\perp} < \chi_{\parallel}$.

This is the starting point for a domain selection strategy. To detect changes in length developing along a fourfold axis, the sample was glued so that a cube's fourfold axis, [001], was aligned with the capacitance sensitive direction. The horizontal plane in which the magnetic field can be rotated was defined by putting the twofold axis [110] horizontal, together with [001]. The expected domain selection and the identification of the detected strain are summarised in Table 2. One observes that all the four quantities sought should be accessed. This obviously relies on the effectiveness of the field in selecting domains. Whether the applied field is strong enough in amplitude to achieve the domain selection is a question which can be solved only experimentally.

The measurements where carried out under constant field while decreasing the temperature from the paramagnetic state. The results of the study are condensed in Fig. 1, which shows, $\lambda_{\parallel} - \lambda_{\perp}$ as a function of the temperature, for various applied fields. One immediately notes the 2 T curve shows lower amplitude for the magnetostriction phenomena than the 4 and 6 T curves. This reflects the imperfect domain selection achieved for this field value. To the contrary, the 4 and 6 T curves are quite similar, demonstrating that total domain selection has been reached. As expected from our prior analysis, the sign of ε_1^{γ} changes while crossing T_R. The right scale of the plot in Fig. 1 gives directly the value of the ordered quadrupolar moment $\langle O_2^0 \rangle$ according to Eq. (1) and using a 4.5×10^{-4} value for B^{γ}/C_0^{γ} (Dr J. Rouchy, unpublished)

3.2. Multipolar X-ray scattering experiments

Two rounds of experiments were performed at the ESRF, BM2 beamline, using the 7-circles goniometer and a closed-cycle helium refrigerator. The results of the first round have been already published elsewhere [11] and we will focus here on the second one. A rather short X-ray wavelength $\lambda = 0.8952$ Å, well above the Neodymium L absorption edges, has been used. To reduce the X-ray photons background and improve the $\boldsymbol{Q}$ resolution, a Ge(111) analyser was mounted in front of the detector. The measurements were performed with a vertical scattering plane, in back scattering conditions.

Table 2
Scheme of determination of the tetragonal strain, in phases I and II, via a magnetic field domain selection

Field direction	Domains 4-fold axes in I	Domains 4-fold axes in II	Strain along [001]
[001]	[100], [010]	[001]	$\lambda_{\perp}$(I), $\lambda_{\parallel}$(II)
[110]	[001]	[100], [010]	$\lambda_{\parallel}$(I), $\lambda_{\perp}$(II)

The [100] surface of the NdMg single crystal was prepared by cleaving. The sample was installed with the [110] direction along the goniometer φ axis. In such conditions, ($hk0$) reflections (h and k positive) could be obtained with same X-rays incident and emerging angles with respect to the crystal surface.

The sample was then cooled down to the minimum available temperature, $T = 18.5$ K, within the temperature range of phase II. As already observed [11], it appeared that the low temperature tetragonal strain was large enough to resolve the peaks associated with the three magnetic domains. In order to detect $(n/2\, m/2\, 0)$ charge satellites, the investigation was restricted to the domain where [0 0 1] is the preserved fourfold axis. The search for the quadrupolar reflections was then organised through (h, k) scans, parallel to the [110] direction, across the expected positions. The accumulated counting time was typically half an hour per point. Fig. 2, shows the result of the scan across the [5/2 3/2 0] position at $T = 18.5$ K together with its equivalent in the paramagnetic range. The quadrupolar peak is clearly defined at 18.5 K and, as expected, is absent at 73 K.

In an attempt at a quantitative analysis, the intensities of the satellites were linearly calibrated after the ones obtained for neighbouring lattice reflections scanned in equivalent conditions. This is a rather delicate approach since there are five orders of magnitude in between the

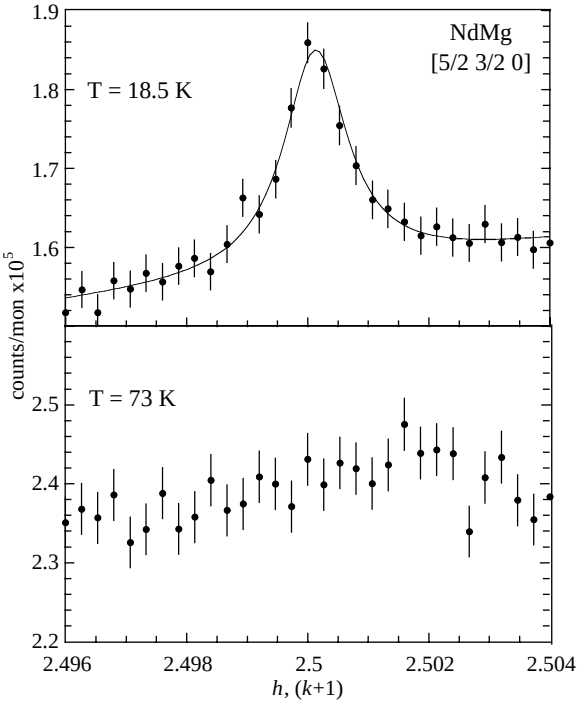

Fig. 2. Upper part: scan along the [110] direction across the [5/2 3/2 0] quadrupolar reflection at $T = 18.5$ K, within the double-k ordered phase of NdMg. The line is a lorenztian + linear background fit to the peak. Lower part: equivalent scan above the Néel temperature at $T = 73$.

two kinds of reflections. In particular, this supposes that the phenomena of extinction, which affects strong reflections, is negligible. Within this assumption, the scattering amplitude for the measured quadrupolar satellites could be defined in terms of Thomson electrons. After Eqs. (2) and (3), in the context of phase II, the theoretical quadrupolar scattering amplitude should read as :

$$A_2(\boldsymbol{Q}) = \alpha_J F_2(Q) 6 \frac{hk}{h^2+k^2+l^2} \langle P_{xy}(\boldsymbol{q}) \rangle. \quad (4)$$

In order to eliminate the dependence on the diffraction indices (h,k,l), the experimental values of scattering amplitude were divided by $hk/h^2+k^2+l^2$ and then plotted versus $\sin\theta/\lambda$ on Fig. 3. Despite the very large error bars, due both to the statistics and to the dispersion of the calibration on lattice reflections, one observes the expected decrease of the amplitude for low scattering angles and the maximum at intermediate angles. To extract a value for the ordered quadrupolar component $\langle P_{xy} \rangle = \pm \langle P_{xy}(\boldsymbol{q}) \rangle$ a fit to the experimental results, using the quadrupolar form factor of Nd^{3+} of Ref. [8], was superimposed to the plot. The fit yields: $\langle P_{xy}(\boldsymbol{q}) \rangle = 2.5 \pm 0.5$.

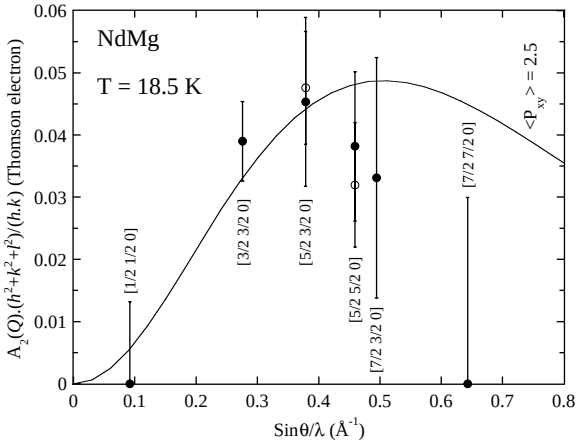

Fig. 3. The quadrupolar scattering amplitude, multiplied by $(h^2+k^2+l^2)/(hk)$, as a function of $\sin\theta/\lambda$. Black dots: The experimental data for the indicated reflections. The open dots are from previous measurements [11]. Solid line: a theoretical curve calculated for $\langle P_{xy} \rangle = 2.5$ after Eq. (4).

The experimental maximum of the form factor appears to be shifted toward lower values of scattering angle with respect to the theoretical one. The most straightforward explanation for this discrepancy is that the theoretical form factor used here is derived from non-relativistic Hartree–Fock wave functions. Accounting for relativistic effects should result in a more spatially extended $4f$ electronic distribution, then in form factors pushed to lower scattering angles [12].

By lack of beam time no diffraction data were collected in phase I. Checking the expected absence of multipolar X-ray peaks for this phase (cf. introduction of this section) would have required to identify again the lattice reflections from three types of tetragonal domains. This, together with the large counting time necessary (at least 20 min per point), would have cost much more time than available. Therefore, it was decided to check the disappearance of the multipolar satellites directly within the paramagnetic phase at $T = 73\,\mathrm{K}$ (for instance, Fig. 2 lower part), with the simplification of a purely cubic lattice.

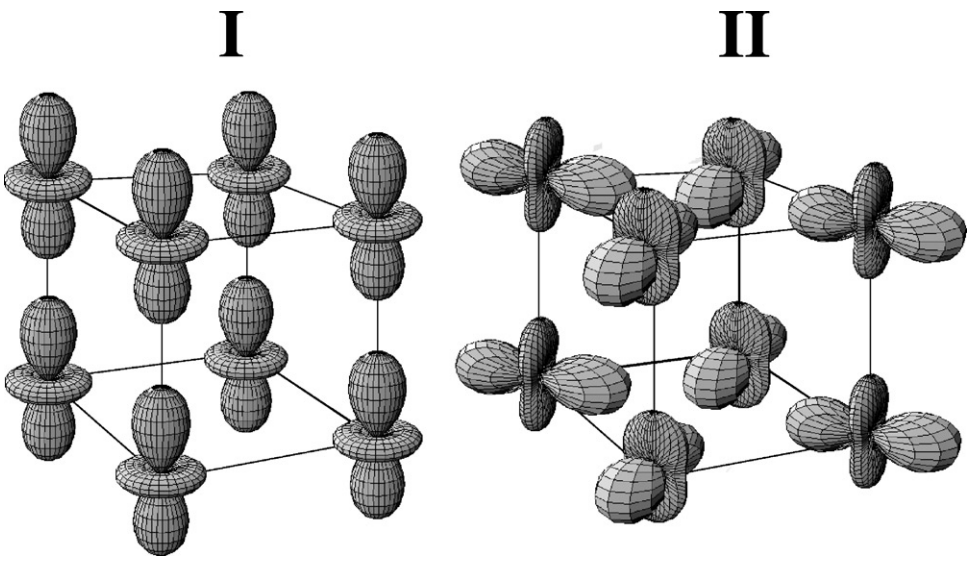

Fig. 4. Sketches of the quadrupolar angular $4f$ distributions in phase I, at $T = 36\,\mathrm{K}$ ($\langle O_2^0 \rangle = 10$), and in phase II, at T=18.5 K ($\langle O_2^0 \rangle = -7$, $\langle P_{xy} \rangle = \pm 2.5$).

4. Discussion

Fig. 4, shows schematic representations of the 4*f* quadrupolar angular distributions in phase I and II, as defined by the experimentally determined values of $\langle O_2^0 \rangle$ and $\langle P_{xy} \rangle$. One has to be aware that the α_J Stevens factor for Nd^{3+} is negative, which means the represented angular electronic densities describe a lack of electrons. To get a more realistic picture, the negative quadrupolar distribution should be combined with the main, positive and spherical, one. Then, in apparent contrast with Fig. 4, the actual angular distribution in phase I would be minimum along the *z*, vertical axis. This type of representation has been chosen because the quadrupolar correction to the spherical situation is a small one; replacing the drawings of Fig. 4 with plots including the spherical term would have resulted in quite unclear sketches.

The main criticism which may be put forward against this study regards the determination of the $\langle P_{xy} \rangle$ value from X-ray measurements with the above-mentioned calibration problem. Theoretical values of $\langle P_{xy} \rangle$ may be computed in a mean field approach, starting from a reasonable crystal field scheme. The obtained values result about two times larger than the experimental one. At this stage, it is impossible to decide in favour of experiment or theory, but the question of defining a calibration method for X-ray reflections five orders of magnitude smaller than typical lattice reflections is to be investigated.

However, regardless of quantitative aspects, X-ray multipolar scattering has been established as an efficient probe of 4*f* distributions which do not respect the initial lattice translations. Such experiments can provide valuable, although indirect, information about the magnetic structure. For instance, in NdMg, the existence of a charge $\langle 1/2\,1/2\,0 \rangle$ wave vector is a proof of the multiaxial nature of phase II. More recently, we used this technique for determining the magnetic structure of TbMg [13].

The quantitative determination of the quadrupolar zone centre components from magnetostriction measurements seems more reliable. Regarding this technique, the main difficulty lies in the definition of a strategy for acting on the domains distribution. This may become very delicate in case of an unknown magnetic structure.

References

[1] G.A. Gehring, K.A. Gehring, Rep. Prog. Phys. 38 (1975) 1.
[2] P.M. Levy, P. Morin, D. Schmitt, Phys. Rev. Lett. 42 (1979) 1417.
[3] P. Morin, D. Schmitt, in: K.H.J. Buschow, E.P. Wohlfarth (Eds.), Ferromagnetic Materials, Vol. 5, North-Holland, Amsterdam, 1990, p. 1.
[4] D. Schmitt, J. Phys. 47 (1986) 677.
[5] K.H.W. Stevens, Proc. Phys. Soc. (London) A 65 (1952) 209.
[6] E. du Trémolet de Lacheisserie, Ann. Phys. 5 (1970) 267.
[7] P. Morin, D. Schmitt, E. du Trémolet de Lacheisserie, Phys. Rev. 21 (1980) 1742.
[8] M. Amara, P. Morin, J. Phys.: Condens. Matter 10 (1998) 9875–9888.
[9] M. Deldem, M. Amara, R.M. Galéra, P. Morin, D. Schmitt, B. Ouladdiaf, J. Phys.: Condens. Matter 10 (1998) 165.
[10] M. Amara, S.E. Luca, R.M. Galera, J. Phys.: Condens. Matter 13 (2001) 9621.
[11] M. Amara, R.M. Galéra, P. Morin, J.F. Bérar, J. Phys.: Condens. Matter 10 (1998) L743.
[12] A.J. Freeman, J.P. Desclaux, J. Magn. Magn. Mater. 12 (1979) 11.
[13] S.E. Luca, M. Amara, R.-M. Galéra, J.-F. Bérar, J. Phys.: Condens. Matter 14 (2002) 935–944.